Long-Distance Demonstration and Modeling of Low-Power Silicon Microdisk Modulators

William A. Zortman, *Student Member, IEEE*, Anthony L. Lentine, *Member, IEEE*, Douglas C. Trotter, and Michael R. Watts, *Member, IEEE*

***Abstract*—Silicon micro-resonators have been proposed for short-distance intracomputer interconnects and recently for long-distance communications. In this letter, the spectral profile, chirp, and power penalties are theoretically analyzed, measured, and compared for a recent silicon microdisk resonator technology. Theory predicts negative pulse chirping of the transmitted wave which when combined with the dispersion properties of SMF-28 fiber results in no power penalty at 40 km and less than 1 dB for 70 km at 5 Gb/s. The measurement at 5 Gb/s agrees with the theoretically predicted values. Measurement of the modulator at a bandwidth limited speed of 10 Gb/s results in 2- and 6.5-dB power penalties at 40 and 70 km, respectively. Comparison with commercial Mach–Zehnder modulator (MZM) technology at 70 km shows that the silicon microdisk is within 0.5-dB power penalty of the MZM at 5 Gb/s and within 4 dB of the MZM power penalty at 10 Gb/s. Theory and experimental results show silicon photonic modulators can be competitive options for long-distance communications.**

***Index Terms*—Networks, resonators, silicon-on-insulator technology, wavelength-division multiplexing.**

I. Introduction

RECENT work in silicon photonics has focused on creating compact filters, modulators and detectors for integration on complimentary metal oxide semiconductor (CMOS) or a photonic chip bonded to CMOS [1]–[4]. Recent measurements of silicon resonant modulators have shown potential for geographically separated interconnects which, among many other applications, could enable long haul/short haul datacenter communication transparency [5], [6]. Previous work [6] does not include a physical model that corroborates with measurements and the short pseudorandom bit sequence (PRBS) of $2^7 - 1$ is not predictive for the commonly used G.709 Optical Transport Channel Unit-2 protocols operating at 10 Gb/s that are approximated more accurately with longer bit sequences. Thus, the shorter bit sequence can potentially lead to less dispersion penalties as measured in [6] than would be achieved in an actual long distance system and less than the measurements that we report here. Here, we measure the long distance dispersion characteristics of low power microdisk technology and in consideration of the application use a more stringent $2^{31} - 1$ PRBS. Results are for the first time substantiated with a resonator model.

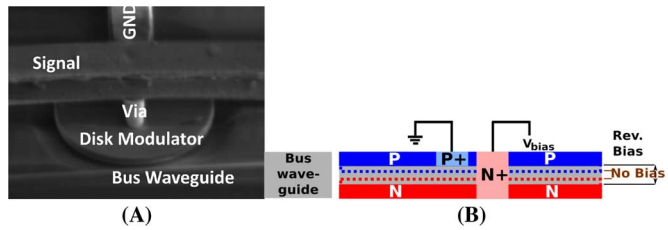

Fig. 1. (a) SEM of the disk modulator. The signal line delaminated from the via during SEM preparation which accounts for its bent appearance. (b) Modulator side view shows it is a vertical depletion device, side coupled to a bus waveguide, and designed to run in reverse bias. P-type doping is on top, N-type on the bottom with highly doped plugs in the center.

The disks are 3.5 μm in diameter, using 240 nm thick silicon on insulator with a 350 nm bus to waveguide separation. Contact is made using tungsten to highly doped P and N ohmic regions with PN junction overlap in a vertical depletion region as depicted in Figs. 1 and 2(a). The advantage of this design is that by using reverse bias modulation in a compact design record low energy/bit is achieved [7] and no pre-emphasis is needed. Furthermore, disks suffer from fewer manufacturing variations than rings because there is no inner radial dimension or etch-depth sensitive super-radial contact area [8]. Modulation here is 3.5 V peak-to-peak reverse bias.

II. Analysis

When considering the long distance transmission, a simple first order phenomenological model for a critically coupled resonator [9] is used to describe the transmitted waves:

$$s_t = \frac{j\left(\omega - \omega_0(t)\right)}{j\left(\left(\omega - \omega_0(t)\right) + \frac{1}{\tau(t)}\right)} s_i \tag{1}$$

where s_i is the source wave amplitude incident at the disk-waveguide point, s_t is the through-port (transmitted) wave amplitude, ω is the frequency of the continuous wave laser line incident on the resonator, ω_0 is the resonant frequency of the disk, and τ is the photon lifetime. Both ω_0 and τ are functions of the voltage

Manuscript received September 20, 2010; revised March 18, 2011; accepted March 26, 2011. Date of publication April 05, 2011; date of current version May 25, 2011. Sandia is a multiprogram laboratory operated by Sandia Corp., a Lockheed Martin Co., for U.S. DOE National Nuclear Security Administration under Contract DE-AC04-94AL85000.

W. A. Zortman is with Sandia National Laboratories, Applied Photonic Microsystems, Albuquerque, NM 87185 USA, and also with the Center for High Technology Materials, University of New Mexico, Albuquerque, NM 87131 USA (e-mail: wzortm@sandia.gov).

A. L. Lentine and D. C. Trotter are with Sandia National Laboratories, Applied Photonic Microsystems, Albuquerque, NM 87185 USA.

M. R. Watts is with the Research Laboratory of Electronics, Massachusetts Institute of Technology, Cambridge, MA 02139 USA (e-mail: mwatts@MIT.edu).

Color versions of one or more of the figures in this letter are available online at http://ieeexplore.ieee.org.

Digital Object Identifier 10.1109/LPT.2011.2138692

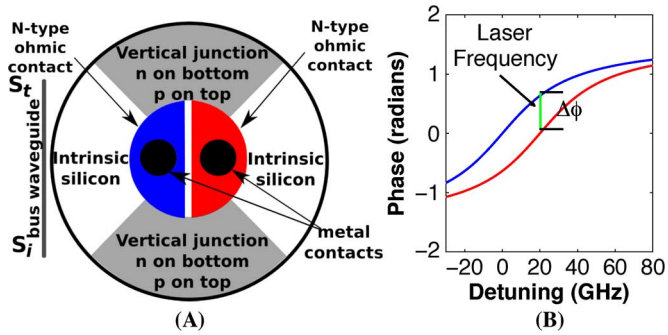

Fig. 2. (a) Top view shows the PN junction covers pi-radians of the disk and the ohmic contacts are half-moon-shaped mirroring the disk circumference. (b) Phase response of the modulator for resonant frequencies detuned 20 GHz from each other. Phase accumulates when moving to lower frequency.

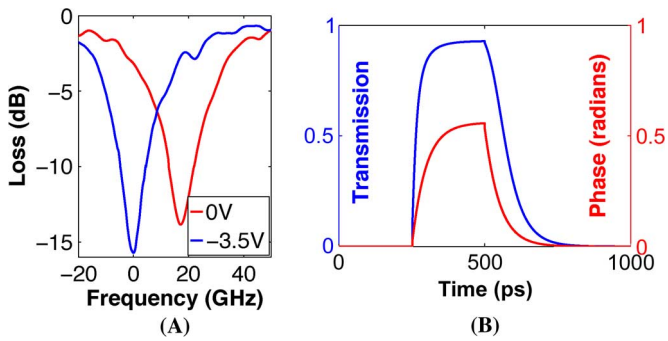

Fig. 3. (a) Resonances for 0- and 3.5-V reverse bias. The source laser is on the resonance for a logic "0" (i.e., +20 GHz on the plot above). (b) The time evolution of the pulse and phase at 5 Gb/s. The phase evolution shows the change from high frequency to low frequency.

across the modulator. Fig. 2(a) shows the incident and transmitted ports, s_i and s_t respectively. For a modulator with no drop waveguide, which is the case here, we are only interested in the transmitted wave. Under modulation this is a pulse with amplitude given by (1) and phase, ϕ, given by the component analysis of (1):

$$\phi = \tan^{-1}\left\{\tau(t)\left[\omega - \omega_0(V)\right]\right\} \tag{2}$$

By inspection of (2) it is clear that when $\omega = \omega_0$ the phase term is zero and that the phase changes to higher values as the resonance (ω_0) moves to lower frequencies away from the laser frequency allowing the laser wave to pass creating a logic "1". This action of the phase can be seen in Fig. 2(b) where the phase response of the modulator is plotted for two different resonances. Movement of ω_0 by 20 GHz results in a phase shift of about 1/2 a radian for constant frequency ω which is the carrier wave emanating from a laser source. Because of the accumulated phase during this operation, higher frequencies are in the pulse leading edge.

To quantify this action, the resonances were measured at 0 V, a logic "0", and −3.5 V, a logic "1". Plots of the resonances of these two states are shown in Fig. 3(a). The 3.5 V reverse bias point shows a higher Q because of the longer photon lifetime possible when carriers are swept out of the disk in reverse bias. The values of the photon lifetime at the two points are estimated using the 3 dB width of the resonance to be 5.2 ps and 5.9 ps for 0 V and −3.5 V respectively. The resonant frequencies and photon lifetimes at these bias points were then used as endpoints for the sweep of ω_0 and τ in (1). To simulate the forcing between these endpoints a time constant was computed from the device series resistance and capacitance to emulate the charge depletion action in the resonator. The pulse and temporal phase as predicted by (1) is depicted in Fig. 3(b). The model also predicts a phase evolution with high frequencies at the front and lower frequencies at the back, which are consistent with the theoretical study done in [10]. The change from higher frequency to lower frequency during the duration of the pulse is evident and this will cause pulse compression in standard SMF-28 fiber which has a dispersion factor of ∼18 ps/nm-km for 1550 nm light. This negates some of the group velocity dispersion for an unchirped Gaussian pulse as will be demonstrated with both theoretical and measured results.

To estimate the resulting power penalties, reference is made to [11] for two equations. (The power penalty in this case refers to the additional optical power, provided by an erbium doped fiber amplifier, needed in the receiver in order to keep the bit error rate constant for an increase in the transmission distance at a given bit rate.) The first predicts the power penalty based on pulse spreading of a Gaussian pulse for given bit-rate, B, dispersion, D, length, L, and laser linewidth, σ_λ:

$$\delta_d = -5\log_{10}\left[1 - (4BLD\sigma_\lambda)^2\right] \tag{3}$$

The model output becomes imaginary when the inner parenthesis grows beyond unity so use of this equation is limited to bit-rates below 6 Gb/s. Equation (4) provides power penalty for chirp alone which we convert to wavelength for λ_c:

$$\delta_c = -10\log_{10}\left[1 - 4BLD\Delta\lambda_c\right] \tag{4}$$

The values for B, L and D are known from the experiment and fiber characteristic given above. σ_λ is estimated to be 3/4 of the bit rate which accounts for the frequency side bands on the amplitude modulated carrier wave. This leaves the chirp, λ_c, which we estimate by integrating the values from Fig. 2(b) over the length of the pulse to get 70 MHz in the frequency domain for the pulse at 5 Gb/s and about twice that at 10 Gb/s.

The results of (3) and (4) are added phenomenologically to account for the two contributors to power penalty. In the regime where high frequencies lead the pulse (2) predicts compression in SMF-28 fiber leading to the analytically predicted penalties in Fig. 4(a) that will be used in comparison to measurement. The expected group velocity dispersion for an unchirped Gaussian is mitigated by the small pulse compression from the chirp. This leads to no power penalty at 40 km for 5 Gb/s and a 1 dB penalty at 70 km that is also consistent with the theoretical values shown in [5]. The chosen transmission distance is arbitrary, as actual systems have widely varying lengths, but typical for tests of this type.

III. Experimental Results

Before looking at the power penalty measured performance at 40 km and 70 km it is necessary to understand the bandwidth limitation of the modulator. Fig. 4(b) shows that no bandwidth limitation exists up to 5 Gb/s for back-to-back operation of the

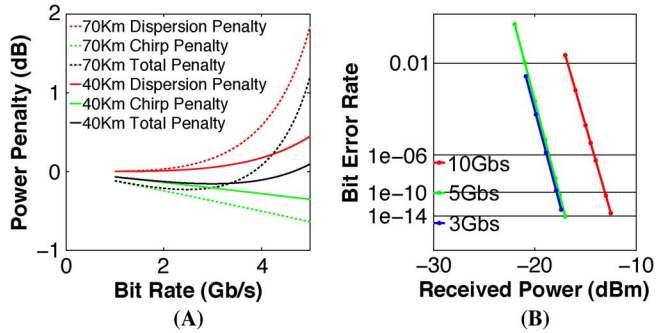

Fig. 4. (a) Predicted power penalties based on (1) bandwidth driven group velocity dispersion alone and (2) chirp, and (3) finally the sum of the two for 40 and 70 km and 5 Gb/s. (b) Probe pad capacitance bandwidth limits the tested device at 10 Gb/s resulting in a back-to-back power penalty at 10 Gb/s.

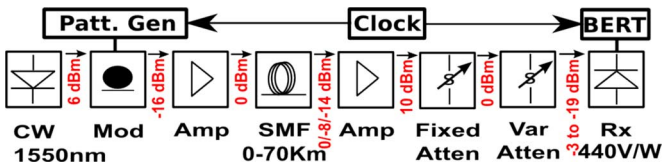

Fig. 5. Experimental setup showing power levels at each stage of the communication system. The signal is amplified before and after the variable length of fiber (0, 40, and 70 km).

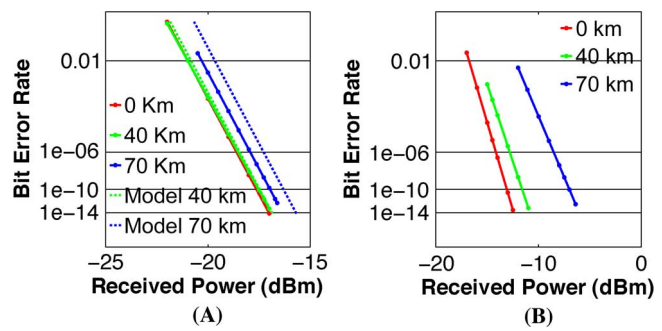

Fig. 6. (a) Measured power penalties for 0, 40, and 70 km at 0, 0, and 1 dB, respectively, at 5 Gb/s are in agreement with theory indicating the modulator benefits in this regime from negative chirp. (b) Bandwidth limitation at 10 Gb/s results in penalties of 1 dB at 40 km and 8.5 dB at 70 km.

modulator and detector. At 10 Gb/s the 0 km bandwidth limitation results from the series resistance and capacitance of the modulator which are 1 $k\Omega$ and $\sim$24 fF (3 dB frequency response $\sim$6.63 GHz). The pad capacitance of 50 fF with 50 Ω impedence has only a small bandwidth impact.

Measurement was done using the setup shown in Fig. 5 with Centellax TG-1B1A pattern generator, clock and bit-error-rate tester (BERT) with $2^{31}-1$ PRBS. Light was coupled from an Agilent 8164B tunable laser into the chip using lensed fibers for total on/off coupling loss of $\sim$20 dB. The signal was amplified before and after the intervening fiber to 0 dBm and then attenuated before the receiver to vary the received power.

Fig. 6 shows the 5 Gb/s data consistent with the model with no power penalty at 40 km. The results at 70 km are also within 0.5 dB of the prediction for a measured penalty of 1 dB. Larger power penalties are observed for 10 Gb/s modulation yet only about 1 dB is seen at 40 km with 6.5 dB at 70 km. Numerical modeling has predicted negatively chirped modulators can achieve <2 dB power penalty at 10 Gb/s and 70 km although the logarithmic nature of (3) precludes analytical prediction beyond about 6 Gb/s [10].

Performance is compared to a lithium niobate Mach–Zehnder Modulator (MZM). The 5 Gb/s performance is within 0.5 dB of the MZM out to 70 km. The MZM shows insignificant penalty at 70 km. The MZM penalty is only 2.5 dB compared to 6.5 dB for the resonator at 10 Gb/s. The 5 Gb/s data and pulse compression modeling in the disk indicate potential for competitive performance at 10 Gb/s with contact redesign.

Silicon photonic microdisk resonators have been demonstrated for long distance applications with a model explaining the low power penalties in the nonbandwidth limited case (5 Gb/s) given. The model predicts 70 MHz of negative chirp in a 200 ps pulse. The negative chirp imposed by the modulator results in pulse compression in SMF-28 fiber which leads to no power penalty at 40 km and 0.5 dB penalty at 70 km. The devices show promise for distributed computing applications with power penalties comparable to installed long distance modulation technology at 5 Gb/s and the potential for similar performance at 10 Gb/s.

REFERENCES

[1] Q. Xu, B. Schmidt, S. Pradhan, and M. Lipson, "Micrometre-scale silicon electro-optic modulator," *Nature*, vol. 435, pp. 325–327, May 19, 2005.

[2] M. R. Watts, D. C. Trotter, and R. W. Young, "Maximally confined high-speed second-order silicon microdisk switches," presented at the Optical Fiber Communication Conf., OSA, San Diego, CA, 2008, Paper PDP14.

[3] A. Alduino, L. Liao, R. Jones, and M. Morse *et al.*, "Demonstration of a high speed 4-channel integrated silicon photonics WDM link with hybrid silicon lasers," presented at the Integrated Photonics Research, Silicon and Nanophotonics, OSA, Monterey, CA, 2010, Paper PDIWI5.

[4] N.-N. Feng, S. Liao, and D. Feng *et al.*, "High speed carrier-depletion modulators with 1.4 V-cm $V_\pi L$ integrated on 0.25 μm silicon-on-insulator waveguides," *Opt. Express*, vol. 18, pp. 7994–7999, 2010.

[5] W. A. Zortman, A. L. Lentine, M. R. Watts, and D. C. Trotter, "Power penalty measurement and frequency chirp extraction in silicon microdisk resonator modulators," in *Proc. Optical Fiber Communication (OFC/NFOEC)*, San Diego, CA, Mar. 21–25, 2010.

[6] A. Biberman, S. Manipatruni, and N. Ophir *et al.*, "First demonstration of long-haul transmission using silicon microring modulators," *Opt. Express*, vol. 18, pp. 15544–15552, 2010.

[7] W. A. Zortman, M. R. Watts, and D. C. Trotter *et al.*, "Low-power high-speed silicon microdisk modulators," presented at the CLEO, San Jose, CA, 2010, Paper CThJ4.

[8] P. Dong, N.-N. Feng, D. Feng, W. Qian, and H. Liang *et al.*, "GHz-bandwidth optical filters based on high-order silicon ring resonators," *Opt. Express*, vol. 18, pp. 23784–23789, 2010.

[9] B. E. Little, S. T. Chu, H. A. Haus, J. Foresi, and J. P. Laine, "Microring resonator channel dropping filters," *J. Lightw. Technol.*, vol. 15, no. 6, pp. 998–1005, Jun. 1997.

[10] L. Zhang, Y. Li, J.-Y. Yang, M. Song, and R. G. *et al.*, "Silicon-based microring resonator modulators for intensity modulation," *IEEE J. Sel. Topics Quantum Electron.*, vol. 16, no. 1, pp. 149–158, Jan./Feb. 2010.

[11] G. P. Agrawal, *Fiber-Optic Communication Systems*, 3rd ed. Hoboken, NJ: Wiley, 2002, p. 210.